Available online at www.sciencedirect.com
ScienceDirect
Solar Energy Materials & Solar Cells 91 (2007) 85–90
Solar Energy Materials and Solar Cells
www.elsevier.com/locate/solmat

Letter

Current routes in polycrystalline $CuInSe_2$ and $Cu(In,Ga)Se_2$ films

Doron Azulay[a], Oded Millo[a,*], Isaac Balberg[a], Hans-Werner Schock[b], Iris Visoly-Fisher[c], David Cahen[c,*]

[a]*Racah Institute of Physics, The Hebrew University of Jerusalem, Jerusalem 91904, Israel*
[b]*Hahn-Meitner-Institut, Berlin, Germany*
[c]*Materials and Interfaces Department, Weizmann Institute of Science, Rehovoth 76100, Israel*

Received 24 July 2006; received in revised form 14 August 2006; accepted 16 August 2006

Abstract

Local electrical transport measurements with scanning probe microscopy on polycrystalline (PX) p-$CuInSe_2$ and p-$Cu(In,Ga)Se_2$ films show that the photovoltaic and dark currents for bias voltages smaller than 1 V flow mainly through grain boundaries (GBs), indicating inversion at the GBs. Photocurrent for higher bias flows mainly via the grains. Based on these results and our finding of ~100 meV GB band bending we deduce the potential landscape around the GBs. We suggest that high grain material quality, leading to large carrier mobilities, and electron–hole separation at the GBs, by chemical and electrical potential gradients, result in the high performance of these PX solar cells.

Keywords: Solar cell; Grain boundaries; Conductive AFM; CIS; CIGS

1. Introduction

Several types of thin-film polycrystalline (PX) solar cells with p-CdTe and chalcopyrites (p-$CuInSe_2$; CIS, and p-$Cu(In_{1-x}Ga_x)Se_2$; CIGS, with $x<0.3$) as absorbers exhibit cell efficiencies that surpass those of the corresponding single-crystal-based devices. This is remarkable as the electrical behavior of PX electronic materials is often interpreted in terms of defects and impurities, which are thought to segregate at the grain boundaries (GBs) and create in-gap localized states that serve as traps. Free charge carriers are then trapped in these GB states, creating a depleted space charge region next to the boundaries, and a potential barrier for electronic transport between adjacent grains [1]. However, for example for CIS, the highest reported single crystal efficiencies are 11–12% [2], compared to empirically optimized ~15% for PX cells (without Ga) [3]. A similar situation holds for CdTe/CdS cells, for which we showed [4,5] that the band bending is strong enough for the GBs to become inverted. As a result, the spatial separation of photo-generated e–h pairs is helped and the minority carriers in the bulk of the grains (electrons here) are channeled along the continuous network of GBs as majority carriers, with minimal e–h recombination [4–7].

These and other possible PX solar cell configurations [6] were considered theoretically already more than 20 years ago [8]. Models, based on GB electrical potential barriers have also been suggested to apply to CIS and CIGS, based on experimental results from various spatially resolved techniques [9–13]. Also a "structural" model for the formation of a hole barrier at the GBs was suggested [14], by assuming that GBs behave as the materials' surfaces, which were earlier [15] found to be Cu-poor (cf. also ref. 12). The presence of Cu vacancies increases the ionization potential, yielding a wider surface bandgap [16], thus forming a barrier for hole transport. Because, in this model, a GB is taken as two adjacent free surfaces, it implies a GB hole barrier, if electrostatic effects are considered [1]. In this case the barrier does not result from electrical charges and was suggested [14] to be beneficial for charge transport, as electrically active defects are usually

*Corresponding authors. Fax: +972 8934 4138.
E-mail addresses: milode@vms.huji.ac.il (O. Millo), david.cahen@weizmann.ac.il (D. Cahen).

0927-0248/$ - see front matter © 2006 Elsevier B.V. All rights reserved.
doi:10.1016/j.solmat.2006.08.006

effective recombination centers, an idea further explored by modeling [17,18]. Hitherto, it has not yet been possible to confirm the predicted (sizeable) GB bandgap widening [12], and one report even suggests some GB bandgap narrowing [19]. We note in passing that in the case of PX CdS, our measurements indicated that GBs actually have a smaller effective band gap than the bulk [20]. Here we present conductive atomic force microscopy (C-AFM) measurements performed on PX CIS and CIGS films, which yield information on the local electrical transport properties of these systems. Our data suggest that the enhanced performance of solar cells based on these PX materials results from the combination of large mobility of both electrons and holes in the grain interiors, and the photocarrier charge separation by chemical and electric potential gradients at the GBs.

2. Experimental

The ~2 μm thick PX CIS and CIGS films were deposited on soda-lime glass substrates, coated by 1 μm thick Mo layer, using the three-stage co-evaporation process, developed for optimal cell efficiencies and described elsewhere. [21–23] With this process no phases that are deleterious for cell performance, such as Cu_xSe, are present in the films. Cross-sectional scanning electron microscopy (Fig. 1) and scanning capacitance microscopy [4] images show that there are several (typically 2–4) grains within the thickness of the studied films, without evidence for other conductive phases. The scanning capacitance measurements also showed that there is no buried homojunction in the structures (at least within the resolution of the method) [4], as will be discussed elsewhere. The Mo layer served as a back contact (counter electrode to the conductive AFM tip) in the C-AFM measurements. The C-AFM data were acquired under either ambient or dry N_2 atmosphere conditions, showing no significant difference.

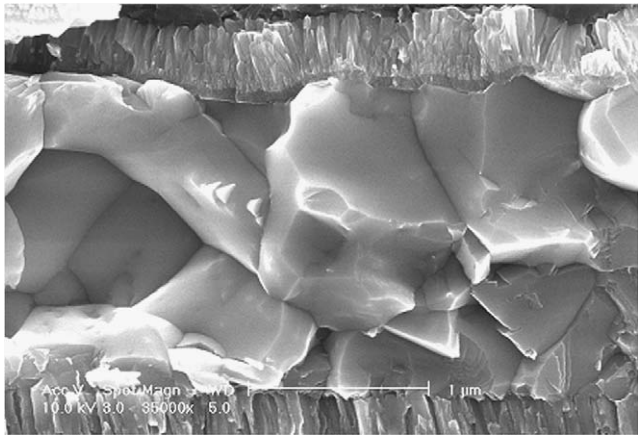

Fig. 1. Cross-sectional scanning electron microscope picture of typical CIGS /CdS sample with, at the bottom, the Mo layer, in the centre the CIGS film and on top the CdS and ZnO. The bar is 1 μm (complete horizontal width of figure is 3.5 μm). Note that the samples used in the present study were without the ZnO and CdS layers.

The tip–sample contact area has a diameter of ~10 nm (based on estimates from the Hertzian model, cf. Ref. [4]). Therefore, with a typical current of 0.1 nA (see below), the current density is ~100 A/cm^2. Since the scan rate was such that the tip stayed locally within the given contact area for less than 1 ms, the electron dose was rather low, of only 10^{18} electrons/cm^2. Consequently, the sample was not damaged in the course of measurements, as manifested by the reproducibility of our topography and current maps.

An original feature in our C-AFM measurements is the ability to acquire simultaneously both dark current and photocurrent images (along with the topography) under identical tip pressure (and electrical contact). This is achieved by implementing a two-pass technique, in which the current in the second pass is measured with the AFM laser turned off (using the stored topographic information gained during the first pass). In this way, the dark and photocurrent measurements are performed on exactly the same location, with identical tip pressure (or electrical contact). This method thus allows separating dark from photo effects also for materials with a bandgap *smaller* than the photon energy of the AFM laser.

The AFM laser intensity (1 mW) is focused to a 100 μm diameter. The light impinges on the tip-sample contact area only after being scattered by the cantilever, as the cantilever shades the tip-sample contact area. As a result only a few percent of the original intensity reaches the relevant area. Considering these two factors leads to an estimated illumination intensity of the order of one to a few suns, comparable to that in operating solar cells. In addition, since the space-charge region width is typically of the order of a few Debye lengths (~100 nm for Debye length of 20–40 nm), also the electric field at the tip/sample interface is similar to that operative in a working solar cell, ~10^4 V/cm.

3. Results and discussion

Fig. 2 shows C-AFM results in the dark (2(a) and (b)) and under AFM laser illumination (2(d) and (e)) at low positive sample bias. The corresponding topographic image in which the grains and GBs are clearly seen is presented in Fig. 2(c). In this low-bias range the dark currents are always positive (i.e., correspond to the bias direction) and are much higher at the GBs than elsewhere. However, under illumination, a *negative photocurrent* (i.e., opposite to the applied bias voltage) flows through the GBs for low enough bias (depicted by the dark regions along the GBs in current image 2(d) and by the red line in the current histogram presented in Fig. 2(f)). This negative current decreases and turns positive in certain GBs at ~100 mV bias, as demonstrated by current image 2(e) and by the blue line in the histogram. By varying the total intensity of the above-bandgap light, using various external light sources (e.g., red and green light lasers), we confirmed that Fig. 2(e) represents the situation under saturated illumination, meaning that the *total* band bending at the GBs is

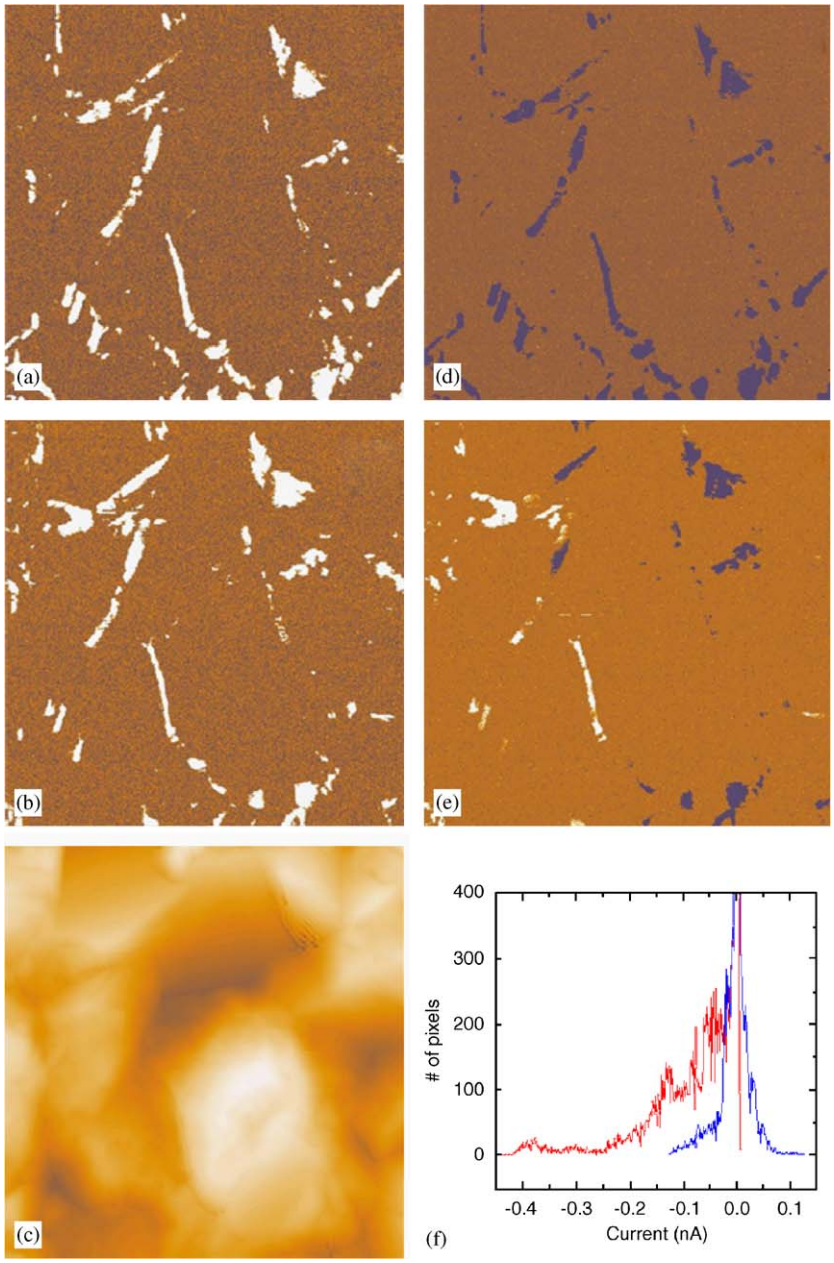

Fig. 2. (a) and (b): Current images in the dark (laser off) at 50 mV (a) and 100 mV (b) of $CuInSe_2$ on Mo films. (c) Topography of the $2 \times 2\,\mu m^2$ area scanned in the current images (color scale range: 300 nm). (d) and (e) Corresponding current images with the laser on, at 50 mV (d) and at 100 mV (e). Note that the dark current is positive in both cases (current ranges: 0.3 nA in (a) and 0.5 nA in (b)) while the photocurrent is negative for bias voltages below 100 mV. (f) Current histograms that give statistical information on the current flowing through the entire scanned area, i.e., for the number of pixels (proportional to the area) at which each current is achieved: red line (negative current only) corresponds to the current image in (d) and blue line (both negative and positive currents) corresponds to the image in (e). C-AFM images were measured using a Solver (NT-MDT) AFM, with Pt-coated tips (Micromesh). Bias polarity is that applied to the sample.

~100 meV. We note that the current is not always seen along the entire GB, and varies somewhat between GBs. This is because of variations among GBs, due to differences in crystallographic orientation, contaminants, tip-GB contact quality and in the series electrical connection with the Mo back contact.

In Fig. 3 we show results from C-AFM experiments under steady (AFM-laser) illumination on CIGS while changing the applied bias along the scan, as indicated by the voltage values shown to the right. These data are also consistent with GB band bending of ~100 meV. Here too, no effect of an additional external light source was seen. We note that this band bending is much less than what we found at CdTe GBs [4]. There, our scanning capacitance microscopy measurements showed that ~500 mV is required for photocurrent sign inversion at the GBs [4,5].

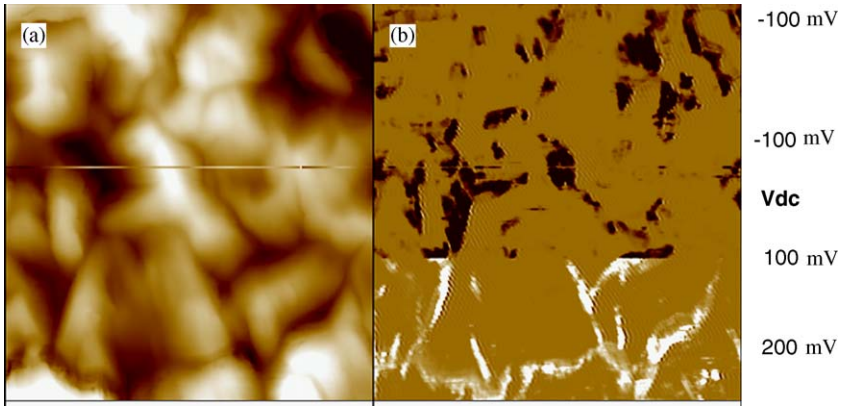

Fig. 3. C-AFM $5 \times 5\,\mu m^2$ measurement performed on a CIGS on Mo film with the AFM laser turned on, while varying the bias voltage during the measurement. The topographic image is presented in (a) and the current image in (b). The voltages were changed along the scan, from top to bottom to values and at positions shown to the right. Note the change in current polarity taking place at $V = 100\,mV$. The images were acquired using a Dimension 3100 (Veeco) AFM, with Pt-coated tips (nanosensors). The photocurrent range is 5 nA.

The observed photocurrents show that there is ~100 mV electric potential difference acting as a photovoltaic (PV) junction at the tip/GB contact. From the lack of a PV effect at the grain surface we deduce that the observed potential difference exists only at the GBs. At the grain surface the corresponding field does not induce observable current, possibly due to faster recombination at the surface than at the GBs, which, thus, are different from the grain surfaces [24,25]. Such GB barriers agree with those deduced from scanning Kelvin probe results [9–11] and with conclusions drawn from macroscopic electrical measurements [26,27] and simulations [17,18].

In contrast to the above results, we found that for high bias voltages ($\geqslant 1$ V) the current through the grains, under illumination, actually exceeds that through the GBs, as shown in Fig. 4. This finding and the fact that the preferred current routes *did not* change with tip pressure, rules out any contact-related artifacts in our current images. More fundamentally, this bias-dependent change in the preferred current routes shows that our results cannot be ascribed to differences between the hole mobilities in the grains and GBs, because, if this would have been the case, the dominant current routes should have been the same at high and low biases [28].

The observation of a higher dark current in the GBs (Fig. 2) can be explained by one of the following scenarios: (1) accumulation of holes in the GBs; (2) depletion of holes but with improved mobility in the GBs (compared to the grain interior); (3) inversion of the dominant carrier at the GBs. (1) is ruled out in view of ample experimental evidence for a hole barrier at the GBs (see e.g., Refs. [10,29]). (2) is very unlikely as it (a) implies an unphysical higher hole mobility at the rather disordered tissue of the GBs than in the grain interior, and (b) being inconsistent with the change of the dominant conduction path with applied voltage (>1 V), as seen in Fig. 4. This leaves scenario **(3)**, which implies a potential landscape around the GBs, as proposed below.

To account for inversion at the GB the energy difference between the conduction band edge, E_c, and the Fermi level, E_F, should a priori be smaller than that between E_F and the valence band edge, E_v. With a typical (E_F—E_v) of ~0.2 eV in these PX materials [17,22] and the 0.1 eV band bending that we find, a valence band offset of the order of about 0.4 eV is needed. Fig. 5 illustrates our suggestion for the corresponding potential landscape in PX CIS and CIGS. We note that such a scenario was proposed previously, based on two-dimensional [18] and one-dimensional modeling [17]. In fact, since it is generally accepted that the electron mobility in these system is an order of magnitude larger than the hole mobility [17,18], electrons can become the dominant carriers in the GBs even without full inversion, reducing the required valence band offset by ~0.1 eV. The corresponding band offset value is now in the range of 0.3 eV, within the range of available theoretical predictions [14,18].

The potential landscape presented in Fig. 5 is consistent with our results that indicate charge separation (and, consequently, preferred current routes) at GBs, even at a bias larger than 0.1 V, i.e., at voltages beyond the band bending deduced from our data. We ascribe this to the hole barrier induced by the valence-band offset at the GBs, as calculated before [14], but which adds to the electrostatic band bending induced by GB defect states [17,18]. Then, at low enough bias, electrons traveling through the grain bulk are more likely to recombine with holes (the majority charge carriers in the grain bulk) than are electrons transported along the GBs.

At very large bias (>1 V) the holes can, by tunneling and field emission, overcome the rather large, yet spatially narrow (a few unit cells) barrier induced by the valence-band offset. The observed large currents that flow through the grains (Fig. 4) are consistent with improved material quality of the grains due to defect segregation at GBs [30]. We note that these high bias conditions are relevant for PV operation of the cell because here the voltage is applied

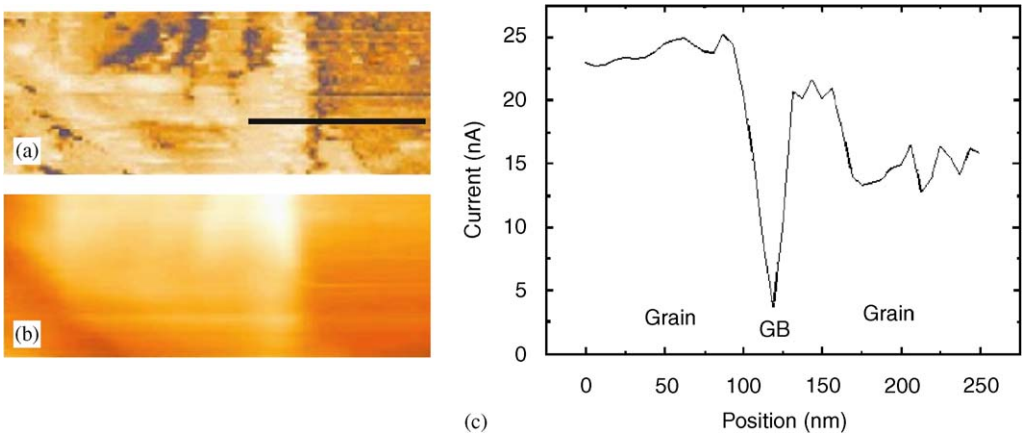

Fig. 4. (a) Current image of PX CIS on Mo film, measured under AFM laser illumination with a bias of 2 V on the $800 \times 300\,nm^2$ area, shown in the topographic image (b). (c) Current variation along the cross-section taken along the line marked in (a). The color scale range in the topographic image is 200 nm.

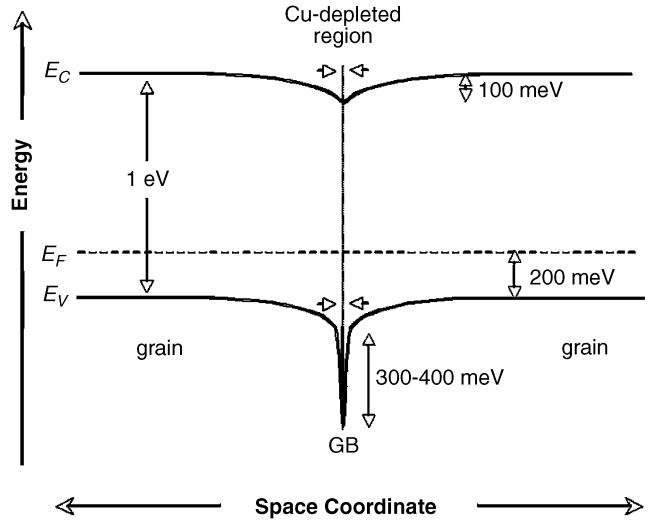

Fig. 5. Suggested schematic potential landscape for $CuInSe_2$ in the vicinity of a GB that can account for dominant electron transport at the GBs in the dark. The (x) length scale is about 0.5–1 μm.

over all of the 2 μm thick absorber film while the PV voltage drops over a fraction of a μm.

The difference we found between the high- and low-voltage behavior helps to understand the fundamental conduction processes in the cell. Since the mobility is not expected to vary significantly with bias voltage, and is likely to be higher in the grains than at and near the GBs, we conclude that the conduction process at higher voltages is dominated by inter-grain transport. This transport process becomes more effective at voltages that are large enough to overcome the inter-grain potential barriers. Once such voltages are exceeded, the system can benefit from the relatively high grain interior mobility, made possible by high intra-grain material quality due to defect migration to the GBs [30]. As described elsewhere, similar experiments with PX CdTe did not reveal such a change in the dominant conduction paths with increasing voltage (up to a few V) [4]. This is consistent with the much larger band bending (~500 meV), and consequently larger barrier to inter-grain transport [5] in the latter system.

4. Conclusion

Our results imply that the mechanism leading to improved solar cell performance in PX CIS- and CIGS-based devices is both similar to, and different from that for the CdTe-based ones. In the latter, it is due to the spatial separation of photo-generated electron–hole pairs, which is induced by the large electrostatic band bending at the GBs, which reduce their recombination rate, at the expense of some loss in open-circuit voltage. In the present case, the photo-generated electron–hole pairs are separated by the electrochemical, i.e., the combined, chemical and electrical, potential gradients around the GB (cf. also ref. 17 for a discussion). In addition, it is likely that the high crystalline purity, leading to large carrier mobility in the grains, as well as the GB-induced partial separation of carriers, are the combined cause for the overall improvement of the photovoltaic behavior in the corresponding solar cells.

The data presented here along with those reported earlier [4–6,9,20] manifest the power of combining various local probe microscopy techniques to understand the electrical properties of PX materials and, thus, to help optimize PX electronic materials in general and PX-based PV devices, in particular. In terms of grain distribution, we repeat our earlier conclusion (for CdTe cells) that the smaller the number of grains that are positioned in between the window and electrode, the better will the cell performance be [4,5]. Clearly, as discussed above, other factors will enter, such as the grain interior quality.

Acknowledgements

This work was supported in part by the Israel Science Foundation (the Jerusalem group) and by the Kimmel Centre for Nanoscale Science (WIS). We thank Dr. S. Cohen, WIS, for introducing us to the two-pass laser on/off

method with the NT-MDT AFM system. DC holds the Schaefer Chair in Energy Research.

References

[1] J.Y.W. Seto, J. Appl. Phys. 46 (1975) 5247.
[2] H.D. Du, C.H. Champness, I. Shih, Thin Solid Films 480–481 (2005) 37.
[3] L. Stolt, J. Hedström, J. Kessler, M. Ruckh, K.O. Velthaus, H.W. Schock, Appl. Phys. Lett. 62 (1993) 597.
[4] I. Visoly-Fisher, Ph.D. Thesis, Weizmann Institute of Science, Rehovot, 2004.
[5] I. Visoly-Fisher, S.R. Cohen, A. Ruzin, D. Cahen, Adv. Mater. 16 (2004) 8793;
I. Visoly-Fisher, S.R. Cohen, A. Ruzin, D. Cahen, Adv. Funct. Mater 16 (2006) 649;
I. Visoly-Fisher, S.R. Cohen, A. Ruzin, D. Cahen, Appl. Phys. Lett. 82 (2003) 1051.
[6] D. Azulay, I. Balberg, V. Chu, J. Conde, O. Millo, Phys. Rev. B 71 (2005) 113304.
[7] O. Breitenstein, M. Langenkamp, J.P. Rakotoniaina, Solid State Phenomena 78–79 (2001) 29.
[8] A.L. Fahrenbruch, R.H. Bube, Fundamentals of Solar Cells: Photovoltaic Solar Energy Conversion, Academic Press, New York, 1983.
[9] D. Fuertes Marron, S. Sadewasser, A. Meeder, T. Glatzel, M.C. Lux-Steiner, Phys. Rev. B 71 (2005) 033306.
[10] C.-S. Jiang, R. Noufi, J.A. AbuShama, K. Ramanathan, H.R. Moutinho, J. Pankow, M.M. Al-Jassim, Appl. Phys. Lett. 84 (2004) 34779.
[11] C.-S. Jiang, R. Noufi, K. Ramanathan, J.A. AbuShama, H.R. Moutinho, M.M. Al-Jassim, Appl. Phys. Lett. 85 (2004) 2625.
[12] M.J. Hetzer, Y.M. Strzhemechny, M. Gao, M.A. Contreras, A. Zunger, L.J. Brillson, Appl. Phys. Lett. 86 (2005) 162105.
[13] M.J. Romero, C.-S. Jiang, R. Noufi, M.M. Al-Jassim, Appl. Phys. Lett. 86 (2005) 143115.
[14] C. Persson, A. Zunger, Phys. Rev. Lett. 91 (2003) 266401;
C. Persson, A. Zunger, Appl. Phys. Lett. 87 (2005) 211904.
[15] R. Herberholz, U. Rau, H.W. Schock, T. Haalboom, T. Goedecke, F. Ernst, C. Beilharz, K.W. Benz, D. Cahen, Eur. J. Appl. Phys 6 (1999) 131.
[16] M.J. Romero, K.M. Jones, J. Abushama, Y. Yan, M.M. Al-Jassim, R. Noufi, Appl. Phys. Lett. 83 (2003) 4731.
[17] K. Taretto, U. Rau, J.H. Werner, Thin Solid Films 480–481 (2005) 8.
[18] M. Gloeckler, J.R. Sites, W.K. Metzger, J. Appl. Phys. 98 (2005) 113704;
W. Metzger, M. Gloeckler, J. Appl. Phys. 98 (2005) 063701.
[19] M.J. Romero, K. Ramanthan, M.A. Contreras, M.M. Al-Jassim, R. Noufi, P. Sheldon, Appl. Phys. Lett. 83 (2003) 4769.
[20] D. Azulay, S. Silbert, O. Millo, I. Balberg, Appl. Phys. Lett. 86 (2005) 212102.
[21] A.M. Gabor, J.R. Tuttle, D.S. Albin, M.A. Contreras, R. Noufi, A.M. Hermann, Appl. Phys. Lett. 65 (1994) 198.
[22] U. Rau, H.-W. Schock, Appl. Phys. A 69 (1999) 131.
[23] U. Rau, D. Braunger, R. Herberholz, H.W. Schock, J.F. Guillemoles, L. Kronik, D. Cahen, J. Appl. Phys. 86 (1999) 497.
[24] In the complete cell, window deposition passivates these exposed grain surfaces.
[25] L. Kronik, U. Rau, J.F. Guillemoles, D. Braunger, H.W. Schock, D. Cahen, Thin Solid Films 361–362 (2000) 353.
[26] R. Chakrabarti, B. Maiti, S. Chaudhuri, A.K. Pal, Sol. Energy Mater. Sol. Cells 43 (1996) 237.
[27] S. Siebentritt, S. Schuler, J. Phys. Chem. Solids 64 (2003) 1621.
[28] Our results reflect the situation at inner GBs (relevant to cell operation), and are not an artifact of sample surface exposure to ambient. This is so because, while the current is measured at the surface, this current has to cross the whole CIS layer between the tip and the Mo back contact. Also measuring under illumination implies that charge carriers are generated well below the surface, from where they are collected by the AFM tip.
[29] S. Sadewasser, T. Glatzel, S. Schuler, S. Nishiwaki, R. Kaigawa, M.C. Lux-Steiner, Thin Solid Films 431–432 (2003) 257.
[30] H.J. Moeller, Semiconductors for Solar Cells, Artech, Boston, 1993.